Effects of pairing correlation on the quasiparticle resonance in neutron-rich Ca isotopes

Ying Zhang [1,2] and Xiao Ying Qu[3,*]

[1]*Department of Physics, School of Science, Tianjin University, Tianjin 300354, China*
[2]*Strangeness Nuclear Physics Laboratory, RIKEN Nishina Center, Wako 351-0198, Japan*
[3]*School of Mechatronics Engineering, Guizhou Minzu University, Guiyang 550025, China*

We investigated the effects of the pairing correlation on the quasiparticle resonant energy and width in the neutron-rich Ca isotopes by using the self-consistent continuum Skyrme Hartree-Fock-Bogoliubov theory with Green's function method. The resonant energy and width can be read from three kinds of quasiparticle spectra, including the quasiparticle-state probability density, the occupation probability density, and the pair probability density. The results read from different quasiparticle spectra calculated with the same potential are exactly the same for the narrow resonances, while for the broad resonances, the difference among the results are relatively larger. From the comparison between the quasiparticle-state probability density calculated with and without the pairing field, we could separate the effect only from the pairing correlation on the quasiparticle resonances. We found that the pairing correlation can increase the resonant energy and width for both the hole-like and particle-like quasiparticle resonances. And this increase is larger when the state is closer to the Fermi energy, especially for the particle-like quasiparticle resonance originated from the unbound single-particle states with smaller angular momentum l in weakly bound nucleus.

I. INTRODUCTION

With the exploration toward the nuclear drip line, people found that the continuum states could play a delicate role in the nucleus far from the β-stability line [1–4]. In these neutron-rich nucleus, since the Fermi energy is very close to the continuum threshold, the pairing correlation could scatter the neutrons to not only the weakly bound orbits but also the continuum states [5–9]. In particular, the low-lying resonant state therein with a small angular momentum l could play an important role in the halo phenomena, due to its extended wave function [7,10]. Moreover, in the collective excitation motion such as the giant resonances, the important contribution of the continuum states mainly comes from the single-particle resonances [11,12].

There have been many theoretical methods which can be used to study the single-particle resonant states in a given nuclear potential based on the mean-field model, such as the R matrix theory [13], scattering phase-shift method [14–19], the Jost function method [20], the real stabilization method (RSM) [21–24], the analytic continuation in the coupling constant method (ACCC) [25–30], and the complex scaling method (CSM) [31–35]. One could also work in the complex momentum representation to search for single-particle resonances [36–39].

On the other hand, since the continuum level density (density of states) is connected to the scattering S matrix, it can be also used to search for the resonances. The level density

can be calculated by the single-particle Green's function for Schrödinger equation [40,41]. Recently, the density of states calculated by the Green's function is used to investigate the single-particle resonance in the relativistic mean-field theory [42,43]. By imposing the proper boundary conditions on the wave functions, the Green's function thus constructed on the complex energy plane can calculate the level density for both the bound and resonant states on the same footing. Besides, the Green's function can be adopted in the CSM [44–46] and combined with the complex momentum representation [47] to investigate the nuclear single-particle resonances.

While approaching the drip line, the single-particle resonances in the mean field could be influenced by the pairing correlation. Conversely, resonances with certain widths could also influence the mean-field and pairing properties of drip-line nucleus. Therefore, it is necessary to describe the resonances in a self-consistent approach which could unify both the mean-filed and pairing correlation. In the mean-field models, the pairing correlation can be treated with Bardeen-Cooper-Schrieffer (BCS) approximation plus Hartree-Fock (HF) approach or the Hartree-Fock-Bogoliubov (HFB) approach. The conventional BCS approximation is not applicable for the neutron-rich nucleus, where the continuum states are involved [5,48]. Therefore, in Refs. [9,10,49,50] the BCS approximation was extended to include the resonant part of continuum through a generalized level density. It is found that the widths of resonant states have an important effect on the pairing properties of nuclei close to the drip line. Besides, the BCS approximation was also applied in the ACCC method [51,52] and the Berggren representation [53–56] to include the resonance states in

_____

*Ketty_Qu@buaa.edu.cn

the mean-field calculations for the description of neutron-rich nuclei. It is worth mentioning that there have been many methods proposed to overcome the drawbacks of the BCS approximation to solve the pairing Hamiltonian in the continuum, such as by using the Richardson solutions [50,57,58] and the configuration-space Monte Carlo approach [59].

The HFB approach in the coordinate space [60,61] is another powerful tool to unify the description of the mean-field and pairing correlations [5,7,48,62–68]. The Bogoliubov quasiparticle resonances have been investigated by several theoretical methods, such as the scattering phase-shift method [69–72], the RSM [73,74], the Jost function method [75], and Gamow HFB method [76]. In particular, with Woods-Saxon type HF and pair potentials, Refs. [71,72,75] investigated the effects of the pairing correlation and the depths of the HF potential on the quasiparticle resonances. Generally speaking, they found that pairing correlation will increase both the resonant energy and width. However, compared at a fixed resonant energy, Ref. [71] found that the pairing correlation has the effect of reducing the width of particle-like quasiparticle resonance in weakly bound nuclei.

Since the Green's function is useful to treat the continuum states, it was also introduced to the HFB theory [77,78]. To take into account the continuum effects on the nuclear properties self-consistently, the Green's function was applied in the HFB theory by using the cutoff local energy-density functional together with gradient pairing force [79], and Skyrme functional with density-dependent delta interaction (DDDI) for pairing [80–82]. Here the HFB Green's function is constructed by the quasiparticle wave functions with the proper boundary conditions for the continuum states. The particle and pair densities are calculated by the HFB Green's function and thus have appropriate asymptotic behaviors to describe the drip-line nuclei. In this way, both the resonant and nonresonant continuum states can contribute to the energy density functional self-consistently. At the same time, the quasiparticle resonance can be identified from the continuum spectral densities [79], or the occupation number density and pair number density [81,83].

In order to further analyze the effects of the pairing correlation on the weakly bound or the resonant single-particle states, the quasiparticle representation could be transformed into the canonical basis which can give better understanding of the level structure. We have done this by diagonalizing the density matrix constructed by the HFB Green's function

[84]. Then, taking the neutron-rich nucleus ^{66}Ca as a numerical example, we investigated the effects of mean-field and pairing correlations on the quasiparticle resonances therein [85]. We found that all the quasiparticle resonances originated from the deeply bound, weakly bound and positive-energy single-particle resonant states, are mainly contributed by the mean-field potential. The pair potential helps to slightly increase the resonant energy and width.

Recently, the neutron-rich Ca isotopes have obtained much attention in the experiment exploration toward the neutron drip line. The new shell closure was found in $A = 52$ and/or $A = 54$ [86–89]. The masses have been measured up to $A = 57$ [86,88]. The newly observed nucleus ^{60}Ca even indicates the existence of ^{70}Ca [90]. Theoretically, the density functional theory with several Skyrme functionals also predicted the drip line of Ca isotopes could be around ^{70}Ca [91]. Considering both the experimental information and global mass models aided by Bayesian machine learning, the two-neutron drip line could be extended up to ^{72}Ca [92].

In this paper, we will further investigate the effects of the pairing correlation on the quasiparticle resonant energy and width within the self-consistent continuum Skyrme HFB theory with Green's function method. Specifically, we will take the neutron-rich Ca isotopes as examples, and investigate the effects of the pairing correlation on quasiparticle resonances originated from different single-particle states as the Fermi energy approaches the continuum threshold. For those particle-like quasiparticle resonances originated from the single-particle resonance in the continuum which already has a width without pairing, we will try to separate the contribution only from the pairing correlation. In Sec. II, the calculation details will be listed. Then the bulk properties of $^{54-66}$Ca, such as the two-neutron separation energy and the canonical single-particle energies will be presented in Sec. III A. The evolution of the quasiparticle spectra, together with the resonant energy and width thus obtained as the Fermi energy approaches the continuum threshold, and as a function of the pairing strength will be discussed in Sec. III B and III C, respectively. Finally, a summary is given in Sec. IV.

II. THEORETICAL METHOD

The HFB theory for finite nuclear system was formulated first in Ref. [61]. In the coordinate space, the HFB equation for the quasiparticle states can be written as [5]

$$\int d\boldsymbol{r}' \sum_{\sigma'} \begin{bmatrix} h(\boldsymbol{r}\sigma, \boldsymbol{r}'\sigma') - \lambda\delta(\boldsymbol{r}-\boldsymbol{r}')\delta_{\sigma\sigma'} & \tilde{h}(\boldsymbol{r}\sigma, \boldsymbol{r}'\sigma') \\ \tilde{h}^*(\boldsymbol{r}\tilde{\sigma}, \boldsymbol{r}'\tilde{\sigma}') & -h^*(\boldsymbol{r}\tilde{\sigma}, \boldsymbol{r}'\tilde{\sigma}') + \lambda\delta(\boldsymbol{r}-\boldsymbol{r}')\delta_{\sigma\sigma'} \end{bmatrix} \phi_i(\boldsymbol{r}'\sigma') = E_i \phi_i(\boldsymbol{r}\sigma), \tag{1}$$

where E_i is the quasiparticle energy, $\phi_i(\boldsymbol{r}\sigma) = [\varphi_{1,i}(\boldsymbol{r}\sigma), \varphi_{2,i}(\boldsymbol{r}\sigma)]^T$ is the corresponding quasiparticle wave function, and λ is the Fermi energy. With Skyrme functionals, the explicit expressions of p-h and p-p single-particle Hamiltonians h and $\tilde{h}$ with the HF potential and pairing potential respectively can be found in Refs. [5,93]. For the

spherical system, the quasiparticle wave function can be represented as

$$\phi_i(\boldsymbol{r}\sigma) = \frac{1}{r}\begin{bmatrix} \varphi_{1,lj}(r) \\ \varphi_{2,lj}(r) \end{bmatrix} Y_{ljm}(\hat{\boldsymbol{r}}\sigma). \tag{2}$$

With the help of the HFB Green's function [77,78], the radial local particle and pair densities can be calculated as [81]

$$\rho(r) = \frac{1}{4\pi r^2} \sum_{lj}(2j+1)\frac{1}{2\pi i} \oint_{C_E} dE \mathcal{G}_{0,lj}^{11}(r,r,E), \quad (3a)$$

$$\tilde{\rho}(r) = \frac{1}{4\pi r^2} \sum_{lj}(2j+1)\frac{1}{2\pi i} \oint_{C_E} dE \mathcal{G}_{0,lj}^{12}(r,r,E), \quad (3b)$$

where $\mathcal{G}_{0,lj}^{11}(r,r,E)$ and $\mathcal{G}_{0,lj}^{12}(r,r,E)$ are "11" and "12" components of the radial HFB Green's functions, respectively. The HFB Green's function is constructed by the quasiparticle wave functions obtained by Eq. (1) with scattering boundary condition for the continuum state with $E > |\lambda|$. As a result, the densities thus obtained have appropriate asymptotic behaviors to describe the extensive density distribution of the nuclei near the drip line [82]. Moreover, the full continuum states, including the resonant states with certain width can contribute to the densities and thus to the energy density functionals self-consistently.

In the calculation, we chose the SLy4 [94] parameter set for the HF mean field and the DDDI for the pairing

field,

$$\Delta(r) = \frac{1}{2}V_0\left[1 - \eta\left(\frac{\rho_q(r)}{\rho_0}\right)^\alpha\right]\tilde{\rho}_q(r), \quad q = n \text{ or } p, \quad (4)$$

where $\rho_q(r)$ and $\tilde{\rho}_q(r)$ are the local particle and pair densities, respectively. The parameter $V_0 = -458.4$ MeV fm^{-3} is chosen together with the energy cutoff $E_{cut} = 60$ MeV to reproduce the neutron-neutron scattering length $a = -18.5$ fm in the free space [95]. The parameters $\eta = 0.71$ and $\alpha = 0.59$ were adjusted for Sn isotopes [96], which can also give the reasonable average pairing gaps for most of the Ca isotopes with SLy4. The angular momentum cutoff is $j = 19/2$. The calculation was carried out with the box size $R = 20$ fm and the mesh size $\Delta r = 0.1$ fm.

To search for the quasiparticle resonance for a given lj partial wave, one could examine the spectrum as a function of the quasiparticle energy, such as the quasiparticle states number density $n_\kappa(E)$, the occupation number density $n_v(E)$, and the pair number density $\tilde{n}_u(E)$ as in Refs. [42,81,82],

$$n_\kappa(E) = \frac{2j+1}{\pi}\text{Im}\int dr\left[\mathcal{G}_{0,lj}^{11}(r,r,-E-i\epsilon) + \mathcal{G}_{0,lj}^{22}(r,r,-E-i\epsilon)\right] \equiv (2j+1)S_\kappa(E), \quad (5a)$$

$$n_v(E) = \frac{2j+1}{\pi}\text{Im}\int dr\, \mathcal{G}_{0,lj}^{11}(r,r,-E-i\epsilon) \equiv (2j+1)S_v(E), \quad (5b)$$

$$\tilde{n}_u(E) = \frac{2j+1}{\pi}\text{Im}\int dr\, \mathcal{G}_{0,lj}^{12}(r,r,-E-i\epsilon) \equiv (2j+1)S_u(E). \quad (5c)$$

The quasiparticle-state probability density $S_\kappa(E)$, occupation probability density $S_v(E)$, and the pair probability density $S_u(E)$ newly defined in the above equations have similar physical meaning as $n_\kappa, n_v, \tilde{n}_u$ but without the degeneracy factor $(2j+1)$.

To plot the quasiparticle spectra for the densities $S_\kappa(E), S_v(E), S_u(E)$, the energy step is taken as $\Delta E = 0.001$ MeV, with a smoothing parameter $\epsilon = 0.005$ MeV to visualize the δ-like peaks for the discrete states and narrow resonances. A quasiparticle resonance could be identified from the peak structure in these spectra if its centroid energy is larger than the quasiparticle continuum threshold $-\lambda$, and its width Γ can be read from the full width of half maximum (FWHM) of the peak subtracting the smoothing value 2ϵ. In addition, to extract the peak centroid energy and the width from the quasiparticle-state probability density S_κ, one has to remove the background of the nonresonant continuum by subtracting the free-particle spectrum calculated with no potentials as in Ref. [42,85].

III. RESULTS AND DISCUSSIONS

In the following discussions, we will take the neutron-rich Ca isotopes as examples to investigate their bulk properties

and the quasiparticle resonances therein, especially the effects of the pairing correlation on these resonances.

A. Properties of neutron-rich Ca isotopes

First, the two-neutron separation energy S_{2n} of $^{48,50,52,...,68}$Ca isotopes calculated by the self-consistent Skyrme HFB theory with Green's function method, and the experimental data [88,97] for $A = 48$–57 are shown in Fig. 1. We found that, with the present interaction SLy4 and DDDI, the calculated two-neutron separation energy is consistent with the experimental data up to $A = 56$, as also shown in Ref. [86]. The largest difference between the theoretical results and the experimental data is around 1 MeV. Our present calculation further shows that the two-neutron drip line is ^{66}Ca, which is lighter than the experimental expectation ^{70}Ca [90] and other theoretical predictions ^{70}Ca [91] or ^{72}Ca [92]. With a close look at the sudden drop of the two-neutron separation energy, the shell closures are found at $A = 48, 52,$ and 60 but not obvious at 54.

In order to have a better understanding of the shell structure, we show the canonical neutron single-particle levels around the Fermi energy within $-10 \sim +10$ MeV for $^{54-66}$Ca in Fig. 2. Obviously, as the neutron number increases, all the levels fall down, but the Fermi energy raises up from
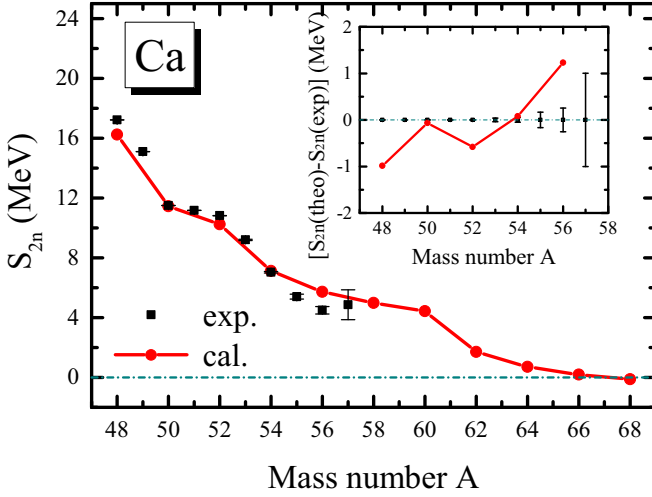
FIG. 1. Two-neutron separation energy S_{2n} of $^{48-68}$Ca isotopes calculated by the self-consistent Skyrme HFB theory with Green's function method. The experimental data [88,97] for $A = 48$–57 are shown as squares. The insert shows the difference between the calculated S_{2n} and the experimental data.

-3.5 MeV to -0.2 MeV. The energy gap $\delta e_{2p} \approx 2$ MeV between $2p_{3/2}$ and $2p_{1/2}$ is comparable with the gap δe_{pf} between $2p_{1/2}$ and $1f_{5/2}$ at $A = 54$. As the neutron number increases, the gap δe_{pf} shrinks obviously, while the gap δe_{2p} remains. The energy gap between $1f_{5/2}$ and $1g_{9/2}$ is nearly 4 MeV and also remains as neutron number increases. Therefore, the shell closure at $A = 60$ is quite prominent.

Below the Fermi energy, the levels $2p_{1/2}$ and $2p_{3/2}$ are bound and occupied. The level $1f_{5/2}$ is bound but above the Fermi energy at $A = 54, 56$. The level $1g_{9/2}$ is not bound up to $A = 62$, and falls into a weakly bound level at $A = 64, 66$, which are quite close to the Fermi energy. More highly above, there are levels $2d_{3/2}$, $2d_{5/2}$, and $3s_{1/2}$. All these
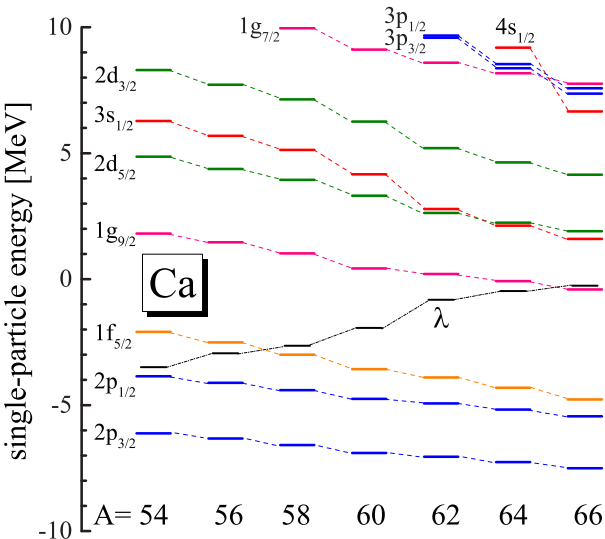

FIG. 2. The neutron single-particle energies for $^{54-66}$Ca around the Fermi energy λ.

single-particle levels are transformed into the Bogoliubov quasiparticle states in the HFB approach.

In Table I, we list the neutron Fermi energy λ and the average pairing gaps $\bar{\Delta}$ for the neutron-rich isotopes $^{54-66}$Ca. For the canonical single-particle states $3s_{1/2}$, $2p_{1/2}$, $2d_{5/2}$, and $1g_{9/2}$ in these nuclei, we list the following information: the top of the HF potential barrier (including the centrifugal potential) V_{max}, the canonical single-particle energy ε_i^{can}, the energy distance between the canonical single-particle energy and the Fermi energy $|\varepsilon_i^{can} - \lambda|$, the state-dependent pairing gap Δ_i, the occupation probability $v_i^2 (= 1 - u_i^2)$, and the factor $u_i v_i$. The occupation probability v_i^2 and the wave function of the canonical basis Φ_i are obtained by diagonalization of the density matrix constructed by the HFB Green's function [84]. The canonical single-particle energy is the expectation value of the single-particle hamiltonian on the canonical wave function $\varepsilon_i^{can} = \langle \Phi_i | h | \Phi_i \rangle$. For the states with $v_i^2 \approx 1$ within the same lj, such as the $1p_{1/2}$ and $2p_{1/2}$ (listed in Table I) states in ^{60}Ca, the single-particle hamiltonian h should be additionally diagonalized in the subspace of these two canonical bases to get the final canonical energy and the wave functions [84]. The state-dependent pairing gap is calculated by $\Delta_i = \langle \Phi_i | \Delta | \Phi_i \rangle$ [93].

The average pairing gaps $\bar{\Delta}$ in $^{54-66}$Ca are all about 1 MeV, except that at the shell closure ^{60}Ca with $N = 40$. On may notice that the average pairing gap $\bar{\Delta} = 0.468$ MeV in ^{60}Ca is a bit large for a closed shell nucleus, obtained by the present pairing parameters $\eta = 0.71$ and $\alpha = 0.59$. We have checked that with a larger η (corresponding to a smaller pairing strength), this average pairing gap will be exactly zero in ^{60}Ca. However, since we mentioned that these parameters $\eta = 0.71$ and $\alpha = 0.59$ can give the reasonable pairing gaps for most of the Ca isotopes, we use them to do the analysis here.

For the canonical state $3s_{1/2}$, its energy is always positive but falls down quickly as the neutron number increases. The state-dependent pairing gap, $\Delta_i \approx 0.7$–0.8 MeV (except ^{60}Ca, and we will not mention this exception in the following discussions), is obviously smaller than the average pairing gap. As this $3s_{1/2}$ level gets closer to the Fermi energy, its occupation probability v_i^2 and $u_i v_i$ increase obviously although it has a positive energy with no centrifugal barrier. This is because the pairing correlation provides the additional attraction to hold neutrons at the $3s_{1/2}$ state in the continuum. For the bound state $2p_{1/2}$, its canonical energy falls from -3.8 MeV to -5.4 MeV, while its barrier top $V_{max} \approx 0.5$ MeV almost unchanged. This level is first close to the Fermi energy, then falls more and more deeply bound. Its occupation probability increases fast and then saturates around 0.98. The level $2d_{5/2}$ always has a positive energy above its barrier top V_{max}. Similarly to the $3s_{1/2}$ state, as it falls down closer to the Fermi energy, its occupation probability v_i^2 and $u_i v_i$ increase obviously. But the state-dependent pairing gap is around 1 MeV, generally larger than that of $3s_{1/2}$. Therefore, at ^{66}Ca, although the level $2d_{5/2}$ is a bit higher than $3s_{1/2}$, its occupation probability is still larger than $3s_{1/2}$. The level $1g_{9/2}$ falls from a positive-energy level to a weakly bound level, which is much below its barrier top $V_{max} \approx 7$ MeV. Its state-dependent

TABLE I. Neutron Fermi energy λ and the average pairing gaps $\bar\Delta$ for $^{54-66}$Ca. For the canonical single-particle states $3s_{1/2}$, $2p_{1/2}$, $2d_{5/2}$, and $1g_{9/2}$, the barrier top of the HF plus centrifugal potential $V_{\max}$, the canonical single-particle energies $\varepsilon_i^{\mathrm{can}}$, the distance between the canonical single-particle energies and the Fermi energy $|\varepsilon_i^{\mathrm{can}} - \lambda|$, the state-dependent pairing gap Δ_i, the occupation probability v_i^2, and the factor $u_i v_i$ are listed. All the values except the factors v_i^2 and $u_i v_i$ are in MeV.

	A	54	56	58	60	62	64	66
	λ	−3.493	−2.939	−2.644	−1.939	−0.817	−0.471	−0.259
	$\bar\Delta$	0.942	1.176	1.116	0.468	1.132	1.237	1.188
$3s_{1/2}$	$\varepsilon_i^{\mathrm{can}}$	6.276	5.687	5.127	4.166	2.788	2.125	1.594
	$|\varepsilon_i^{\mathrm{can}} - \lambda|$	9.769	8.626	7.771	6.105	3.920	2.596	1.853
	Δ_i	0.722	0.863	0.809	0.332	0.758	0.802	0.742
	v_i^2	0.0013	0.0025	0.0027	0.0007	0.0107	0.0223	0.0359
	$u_i v_i$	0.0368	0.0498	0.0518	0.0271	0.1029	0.1475	0.1859
$2p_{1/2}$	$V_{\max}$	0.552	0.536	0.522	0.510	0.504	0.495	0.486
	$\varepsilon_i^{\mathrm{can}}$	−3.856	−4.137	−4.408	−4.756	−4.936	−5.176	−5.447
	$|\varepsilon_i^{\mathrm{can}} - \lambda|$	0.363	1.198	1.764	2.817	4.119	4.705	5.188
	Δ_i	0.886	1.065	1.008	0.429	1.093	1.232	1.219
	v_i^2	0.6895	0.8702	0.9341	0.9943	0.9833	0.9837	0.9867
	$u_i v_i$	0.4627	0.3360	0.2482	0.0754	0.1283	0.1267	0.1144
$2d_{5/2}$	$V_{\max}$	1.950	1.895	1.850	1.808	1.782	1.754	1.725
	$\varepsilon_i^{\mathrm{can}}$	4.859	4.374	3.942	3.309	2.626	2.242	1.906
	$|\varepsilon_i^{\mathrm{can}} - \lambda|$	8.352	7.313	6.586	5.248	3.443	2.713	2.165
	Δ_i	0.854	1.027	0.964	0.401	0.977	1.083	1.060
	v_i^2	0.0026	0.0049	0.0053	0.0015	0.0190	0.0356	0.0509
	$u_i v_i$	0.0508	0.0695	0.0724	0.0381	0.1365	0.1854	0.2199
$1g_{9/2}$	$V_{\max}$	7.956	7.747	7.565	7.402	7.298	7.189	7.087
	$\varepsilon_i^{\mathrm{can}}$	1.809	1.462	1.023	0.426	0.203	−0.081	−0.408
	$|\varepsilon_i^{\mathrm{can}} - \lambda|$	5.302	4.401	3.667	2.365	1.020	0.390	0.149
	Δ_i	1.137	1.407	1.327	0.553	1.354	1.495	1.452
	v_i^2	0.0111	0.0238	0.0298	0.0131	0.1991	0.3736	0.5510
	$u_i v_i$	0.1048	0.1523	0.1701	0.1139	0.3994	0.4838	0.4974

pairing gap $\Delta_i \approx 1.1$–1.4 MeV is generally larger than others. In the following, we will take these canonical states near the Fermi energy as examples to investigate their corresponding quasiparticle spectra, especially the pairing effects therein.

B. Evolution of quasiparticle resonance as Fermi energy

In Figs. 3–6, we show the neutron quasiparticle spectra respectively for $s_{1/2}$, $p_{1/2}$, $d_{5/2}$, $g_{9/2}$ partial waves in the neutron-rich nuclei ^{54,60,62,66}Ca within the energy interval $E = 0$–10 MeV, including the quasiparticle-state probability density S_κ, the occupation probability density S_v and the pair probability density S_u. These spectra are calculated by the HFB Green's function as in Eqs. (5) with both the HF and pair potentials (denoted by the "HFB spectrum" for short in the following), only with HF potential (denoted by the "HF spectrum"), only with pair potential (denoted by the "pair spectrum") and with no potentials (denoted by the "free-particle spectrum"). In the occupation probability density S_v and the pair probability density S_u, the free-particle spectrum is zero since the neutrons are impossible to stay at one state and make pairs there without any potentials. Similarly, in the pair probability density S_u, the HF spectrum is zero since neutrons cannot make pairs without pair potential.

In Figs. 3–6, one could recognize some sharp peak structures which may correspond to quasiparticle resonances. In Table II, we list the peak centroid energies and the widths read from the three densities S_κ, S_v, S_u, respectively, for $p_{1/2}$, $d_{5/2}$, $g_{9/2}$ partial waves in $^{54-66}$Ca. More explicitly, the peak centroid energy (width) read from the HFB spectrum and the HF spectrum of the quasiparticle-state probability density S_κ are $E_{\mathrm{HFB}}^\kappa(\Gamma_{\mathrm{HFB}}^\kappa)$ and $E_{\mathrm{HF}}^\kappa(\Gamma_{\mathrm{HF}}^\kappa)$, respectively. The difference between the widths $\Gamma_{\mathrm{HFB}}^\kappa$ and $\Gamma_{\mathrm{HF}}^\kappa$ should be contributed only from the pairing correlation, so we denote it as $\Delta\Gamma_{\mathrm{pair}}^\kappa$ in the following. Those read from the peaks (if there is) in the occupation probability density S_v are $E_{\mathrm{HFB}}^v(\Gamma_{\mathrm{HFB}}^v)$ and $E_{\mathrm{HF}}^v(\Gamma_{\mathrm{HF}}^v)$, together with the width difference $\Delta\Gamma_{\mathrm{pair}}^v$. In the pair probability density S_u, since there is no HF spectrum, we list only the results read from the HFB spectrum $E_{\mathrm{HFB}}^u(\Gamma_{\mathrm{HFB}}^u)$.

1. Unbound $s_{1/2}$ states

First, from Fig. 3 for the $s_{1/2}$ partial wave, we can see that the absolute value of the density of quasiparticle states S_κ is 10 times larger than those of the occupation probability density S_v and the pair probability density S_u. But in the density S_κ, there is a large contribution from the continuum background near the threshold $-\lambda$, where the free-particle spectrum suddenly appears. In contrast, the densities S_v and S_u do not have such free-particle background. One may notice
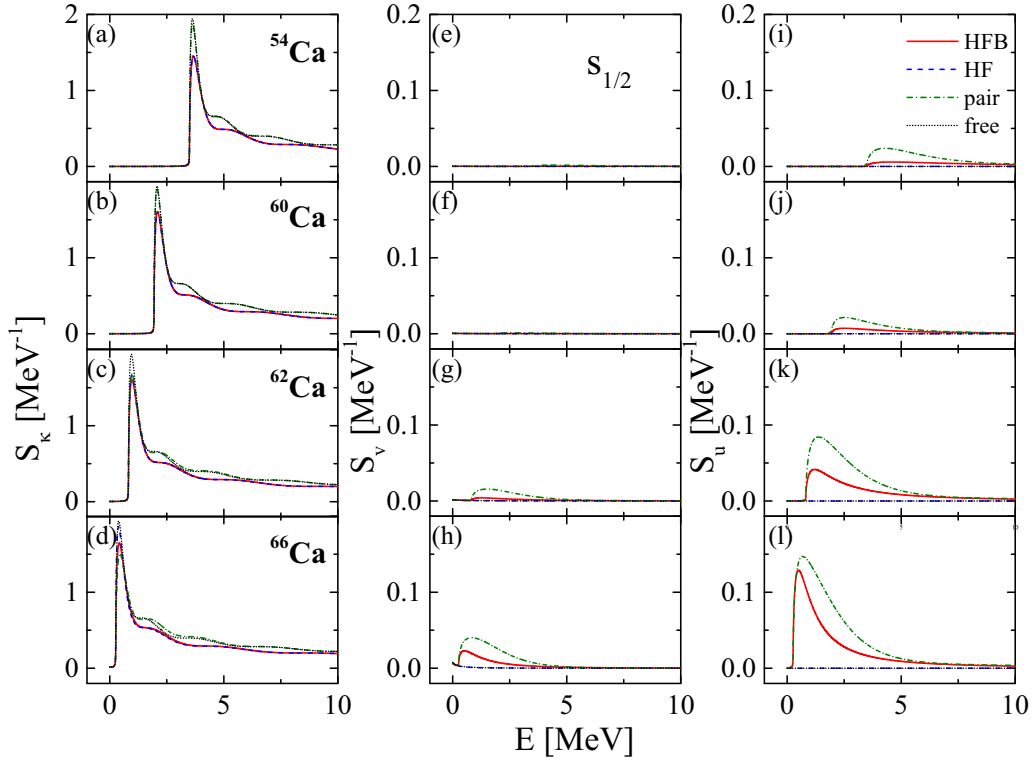
FIG. 3. Neutron quasiparticle spectra for $s_{1/2}$ partial wave in the neutron-rich nuclei ^{54,60,62,66}Ca within the energy interval $E = 0$–10 MeV, including the quasiparticle-state probability density S_κ [(a)–(d)], the occupation probability density S_v [(e)–(h)], and the pair probability density S_u [(i)–(l)]. The spectra are calculated by the HFB Green's function with both the HF and pair potentials (solid line), only with the HF potential (dashed line), only with the pair potential (dash-dotted line), and with no potentials (dotted line).

that the free-particle background in S_κ is even larger than other spectra near the threshold. It was explained in Ref. [42] that this large peak of free-particle spectrum near the threshold could be related to the divergent behavior of the density of states $n(\varepsilon) = \frac{L}{\pi\hbar}\sqrt{\frac{m}{2\varepsilon}}$ when $\varepsilon \to 0$ for free-particle moving in one dimension box $[0, L]$. This much larger free-particle background around the threshold is also found in the $p_{1/2}$ partial wave later but not in $d_{5/2}$ and $g_{9/2}$ partial waves where there are resonances near the threshold.

One can see from S_κ in Figs. 3(a)–3(d) that the quasiparticle continuum threshold $-\lambda$ approaches zero as the neutron number increases. From these spectra shown within 0–10 MeV, we cannot recognize any resonances in the quasiparticle-state probability density S_κ after subtracting the free-particle background. The state $3s_{1/2}$ listed in Table I is one of the canonical states with positive energies, not corresponding to any quasiparticle resonance with the pairing correlation. In spite of this, we can see a bump (not symmetric peak) in the HFB spectra of S_v and S_u near the threshold $-\lambda$ in Figs. 3(e)–3(l). This shows that as the neutron number increases and the Fermi energy approaches zero, more neutrons could be scattered to the continuum in the $s_{1/2}$ partial wave near the threshold and make pairs there. It is impossible without pairing correlation since the HF spectra therein are exactly zero. This is consistent with the increasing occupation probability v_i^2 and u_iv_i found in the $3s_{1/2}$ state as listed in Table I. Moreover, it is interesting to see from the pair spectra of S_v and S_u that, even with only pair potential (e.g., in the

asymptotic region where the mean-field potential almost vanishes, but the pair potential may retain), there could also be neutron pairs in the quasiparticle continuum in the $s_{1/2}$ partial wave near the threshold. And this is more obvious when the Fermi energy approaches zero.

Actually, the resonant-like increase of occupation in the s wave near the continuum threshold was first observed in Ref. [69], then discussed in detail in Ref. [98], and also found in d wave in Ref. [99]. This has an important implication that the low-lying nonresonant continuum can contribute to the formation of the ground state of the weakly bound nucleus.

2. Bound $2p_{1/2}$ state

For the $p_{1/2}$ partial wave, let us first focus on the quasiparticle-state probability density S_κ in ^{54}Ca shown in Fig. 4(a). We can see that the quasiparticle continuum threshold $-\lambda$ is around 3 MeV. There is a sharp peak in the HFB spectrum before this threshold. After subtracting the free-particle background, we could read the peak centroid energy and the width $E_{HFB}^\kappa(\Gamma_{HFB}^\kappa) = 0.936(0.001)$ MeV as listed in Table II. Since the centroid energy is smaller than the threshold $-\lambda$, this peak represents a discrete (bound) quasiparticle state. Actually, this discrete quasiparticle state originates from the bound $2p_{1/2}$ close to the Fermi energy as shown in Fig. 2 and Table I. The width is not exactly zero for such a discrete quasiparticle state, since the energy step to plot the spectra is $\Delta E = 0.001$ MeV, which may induce an uncertainty in width

TABLE II. Peak centroid energies E and widths Γ obtained from the quasiparticle spectra of the partial waves $p_{1/2}$, $d_{5/2}$, $g_{9/2}$ within the energy region $E = 0$–10 MeV for $^{54-66}$Ca. $E_{\mathrm{HF}}^{\kappa}(\Gamma_{\mathrm{HF}}^{\kappa})$ and $E_{\mathrm{HFB}}^{\kappa}(\Gamma_{\mathrm{HFB}}^{\kappa})$ are read from the HF and HFB spectrum of the quasiparticle-state probability density S_{κ} respectively. $E_{\mathrm{HF}}^{v}(\Gamma_{\mathrm{HF}}^{v})$ and $E_{\mathrm{HFB}}^{v}(\Gamma_{\mathrm{HFB}}^{v})$ are those read from the occupation probability density S_{v}, and $E_{\mathrm{HFB}}^{u}(\Gamma_{\mathrm{HFB}}^{u})$ from the pair probability density S_{u}. The columns $\Delta\Gamma_{\mathrm{pair}}^{\kappa}$ and $\Delta\Gamma_{\mathrm{pair}}^{v}$ list the difference between the widths read from the HF and HFB spectrum of S_{κ} and S_{v}, contributed only from the pairing correlation. All the quantities are in MeV.

		S_{κ}			S_{v}			S_{u}
		$E_{\mathrm{HF}}^{\kappa}(\Gamma_{\mathrm{HF}}^{\kappa})$	$E_{\mathrm{HFB}}^{\kappa}(\Gamma_{\mathrm{HFB}}^{\kappa})$	$\Delta\Gamma_{\mathrm{pair}}^{\kappa}$	$E_{\mathrm{HF}}^{v}(\Gamma_{\mathrm{HF}}^{v})$	$E_{\mathrm{HFB}}^{v}(\Gamma_{\mathrm{HFB}}^{v})$	$\Delta\Gamma_{\mathrm{pair}}^{v}$	$E_{\mathrm{HFB}}^{u}(\Gamma_{\mathrm{HFB}}^{u})$
$p_{1/2}$	^{54}Ca	0.362(0.001)	0.936(0.001)	0.000	0.362(0.001)	0.936(0.001)	0.000	0.936(0.001)
	^{56}Ca	1.175(0.000)	1.567(0.001)	0.001	1.175(0.001)	1.567(0.001)	0.000	1.567(0.001)
	^{58}Ca	1.764(0.001)	2.015(0.001)	0.000	1.764(0.001)	2.015(0.001)	0.000	2.015(0.001)
	^{60}Ca	2.816(0.001)	2.845(0.006)	0.005	2.816(0.001)	2.845(0.006)	0.005	2.845(0.006)
	^{62}Ca	4.119(0.001)	4.260(0.037)	0.036	4.119(0.001)	4.260(0.037)	0.036	4.260(0.037)
	^{64}Ca	4.705(0.001)	4.866(0.032)	0.031	4.705(0.001)	4.866(0.032)	0.031	4.866(0.032)
	^{66}Ca	5.188(0.001)	5.332(0.020)	0.019	5.188(0.001)	5.332(0.020)	0.019	5.332(0.020)
$d_{5/2}$	^{54}Ca	5.718(1.418)	5.739(1.402)	−0.016	—	5.846(2.419)	—	5.810(2.150)
	^{56}Ca	5.023(1.524)	5.064(1.500)	−0.024	—	5.092(1.978)	—	5.067(1.854)
	^{58}Ca	4.556(1.534)	4.610(1.536)	0.002	—	4.601(1.670)	—	4.581(1.572)
	^{60}Ca	3.582(1.446)	3.603(1.457)	0.011	—	3.643(1.404)	—	3.636(1.233)
	^{62}Ca	2.246(1.307)	2.467(1.422)	0.115	—	2.489(1.172)	—	2.477(1.153)
	^{64}Ca	1.744(1.020)	2.002(1.316)	0.296	—	2.064(1.036)	—	2.053(1.033)
	^{66}Ca	1.406(0.699)	1.647(1.119)	0.420	—	1.737(0.880)	—	1.729(0.881)
$g_{9/2}$	^{54}Ca	5.009(0.006)	5.122(0.007)	0.001	—	5.122(0.008)	—	5.122(0.008)
	^{56}Ca	4.174(0.003)	4.382(0.005)	0.002	—	4.382(0.005)	—	4.382(0.005)
	^{58}Ca	3.500(0.002)	3.722(0.002)	0.000	—	3.722(0.002)	—	3.722(0.002)
	^{60}Ca	2.288(0.001)	2.350(0.001)	0.000	—	2.350(0.001)	—	2.350(0.001)
	^{62}Ca	0.992(0.001)	1.656(0.001)	0.000	—	1.656(0.001)	—	1.656(0.001)
	^{64}Ca	0.377(0.001)	1.519(0.002)	0.001	0.377(0.001)	1.519(0.002)	0.001	1.519(0.002)
	^{66}Ca	0.155(0.001)	1.442(0.002)	0.001	0.155(0.001)	1.442(0.002)	0.001	1.442(0.002)

reading. The HF spectrum of the density S_{κ} also shows a sharp peak before the threshold $-\lambda$, whose centroid energy and width is $E_{\mathrm{HF}}^{\kappa}(\Gamma_{\mathrm{HF}}^{\kappa}) = 0.362(0.001)$ MeV. It is interesting to notice that this centroid energy is almost the same with the energy distance between the corresponding canonical state and the Fermi energy $|\varepsilon_{i}^{\mathrm{can}} - \lambda| = 0.363$ MeV as listed in Table I. This is easy to understand that, according to the BCS approximation $E = \sqrt{(\varepsilon - \lambda)^2 + \Delta^2}$, without the pairing gap ($\Delta = 0$), the quasiparticle energy is just the shifted single-particle energy ε by $E = |\varepsilon - \lambda|$. The further shift of the peak centroid energy from HF to HFB spectra could be also understood by the BCS approximation due to the addition of Δ. This demonstrates that the BCS approximation works well for such a bound single-particle state and the corresponding quasiparticle state.

Similarly, from Fig. 4(e) we can also see two peaks in the HF and HFB spectra of the occupation probability density S_{v}, which means that once with the HF potential, this state could be always occupied. Indeed, it corresponds to the bound single-particle state $2p_{1/2}$ below the Fermi energy as we mentioned. The peak centroid energy read from the HF and HFB spectra of S_{v} listed in Table II are exactly the same as those read from S_{κ}. In Fig. 4(i) for the pair probability density S_{u}, only the HFB spectra has a sharp peak. This peak centroid energy is also the same as those read from the HFB spectra of S_{κ} and S_{v}.

As the neutron number increases, the sharp peaks in the three densities shifts to the higher energy region, while the quasiparticle continuum threshold $-\lambda$ moves toward zero. In nucleus ^{60}Ca, as shown in Fig. 4(b), the peak of S_{κ} has passed through the threshold $-\lambda$. The peak centroid energy and the width read from the HF and HFB spectra are $E_{\mathrm{HF}}^{\kappa}(\Gamma_{\mathrm{HF}}^{\kappa}) = 2.816(0.001)$ MeV and $E_{\mathrm{HFB}}^{\kappa}(\Gamma_{\mathrm{HFB}}^{\kappa}) = 2.845(0.006)$ MeV, respectively. Both the centroid energies are larger than the threshold $-\lambda = 1.9$ MeV, denoting that they are now quasiparticle resonant states. One should notice that, the single-particle state $2p_{1/2}$ is still bound below the Fermi energy, so the corresponding quasiparticle resonance is a "hole-like" quasiparticle resonance [71]. In this case, the width read from the HFB spectra $\Gamma_{\mathrm{HFB}}^{\kappa}$ should be contributed only from the continuum coupling due to the pairing correlation. One can see that the width $\Delta\Gamma_{\mathrm{pair}}^{\kappa} = 0.005$ MeV is rather small, since the average pairing gap $\bar{\Delta} = 0.5$ MeV is quite small in this closed shell nucleus ^{60}Ca. As discussed in Ref. [71], for a hole-like quasiparticle resonance, its width is proportional to the average pairing gap $\bar{\Delta}^2$ according to the Fermi's golden rule. From the occupation probability density S_{v} and the pair probability density S_{u} shown in Figs. 4(f) and 4(j), exactly the same quasiparticle resonant energy and width can be read from their HFB spectra, as listed in Table II. This shows that, for such a narrow hole-like quasiparticle resonance, the three kinds of densities
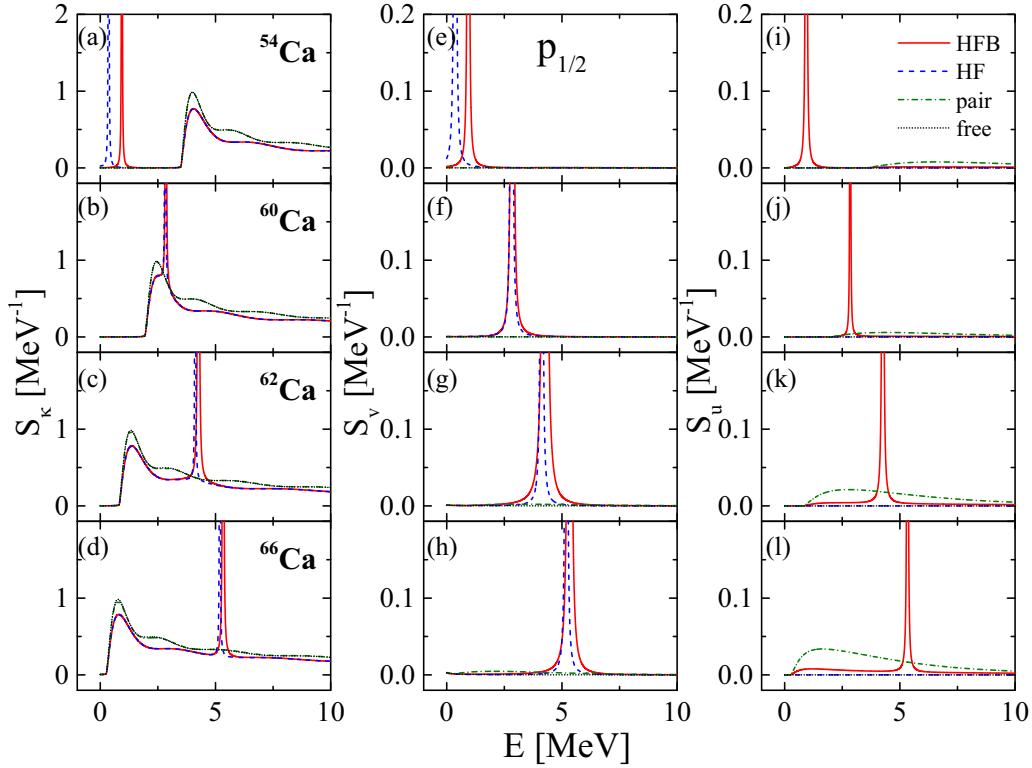
FIG. 4. Similar to Fig. 3 but for $p_{1/2}$ partial wave.

S_κ, S_v, and S_u calculated with the same potential can provide the same resonant energy and width.

With more and more neutrons in $^{62-66}$Ca, the peak of the HFB spectra in the $p_{1/2}$ partial wave in the densities S_κ, S_v, and S_u moves higher and higher above the quasiparticle continuum threshold. The corresponding widths contributed only from the pairing correlation in ^{62,64,66}Ca are $\Delta\Gamma^{\kappa,v}_{\text{pair}} = 0.036, 0.031, 0.019$ MeV respectively read from the densities S_κ and S_v. These widths are obviously larger than that in ^{60}Ca, since their average pairing gap $\bar{\Delta} \approx 1.0$ MeV are much larger. Among these three nuclei, ^{62,64}Ca have relatively larger $\Delta\Gamma^{\kappa,v}_{\text{pair}}$ than ^{66}Ca. Meanwhile, we found that the occupation probability factors $u_i v_i$ of the $2p_{1/2}$ states in ^{62,64}Ca are also larger than that in ^{66}Ca. It is easy to know that, for a fully occupied state or an exactly empty state far away from the Fermi energy, the factor $u_i v_i$ should have the smallest value 0, and such states will not be affected by the pairing correlation according to the BCS theory. While, the largest value of $u_i v_i$ corresponds to the half-occupied state with $v_i^2 = u_i^2 = 0.5$ closest to the Fermi energy, where the pairing correlation is the most effective. Therefore, the hole-like quasiparticle resonance originated from the bound single-particle state with larger $u_i v_i$ and closer to the Fermi energy could have a larger width contributed from the pairing correlation.

Besides, from the pair probability density S_u in the $p_{1/2}$ partial wave in ^{62,66}Ca shown in Figs. 4(k) and 4(l), it is interesting to see that, even with only pair potential, the pair probability density S_u above the quasiparticle continuum threshold obviously grows as the threshold approaches zero. This is similar to what we found in $s_{1/2}$ partial wave shown

in Figs. 3(k) and 3(l). This fact indicates that, the continuum coupling effect near the threshold due to the pairing correlation also happens in the $p_{1/2}$ partial wave, but to a less extent than that in the $s_{1/2}$ partial wave.

3. Unbound $2d_{5/2}$ state

The quasiparticle spectra shown in Fig. 5 for the $d_{5/2}$ partial wave are quite different from those for $p_{1/2}$ in Fig. 4. It is difficult to recognize any peaks from the quasiparticle-state probability density S_κ due to the free-particle background in Figs. 5(a)–5(d). It is also difficult to see any peaks in the occupation probability density S_v in ^{54,60}Ca in Figs. 5(e) and 5(f) due to the small spectrum value. But the density S_v in ^{62,66}Ca in Figs. 5(g) and 5(h), as well as the pair probability density S_u in Figs. 5(i)–5(l), clearly show that there is a peak structure above the quasiparticle continuum threshold, which represents a quasiparticle resonance. This quasiparticle resonance originates from the unbound single-particle $2d_{5/2}$ above the Fermi energy, so it is a "particle-like" resonance according to Ref. [71]. It cannot be occupied at all only with the HF potential. So there is no HF spectrum in the occupation probability density S_v in Figs. 5(e)–5(h). Even with the pairing correlation, the HFB spectrum in S_v is almost invisible in ^{54,60}Ca, since the single-particle state $2d_{5/2}$ is too high above in the continuum to be scattered to by the pairing correlation. As the neutron number increases and the state $2d_{5/2}$ falls down closer to the Fermi energy, the peak corresponding to this quasiparticle resonance in the density S_u becomes higher and narrower in Figs. 5(i)–5(l).
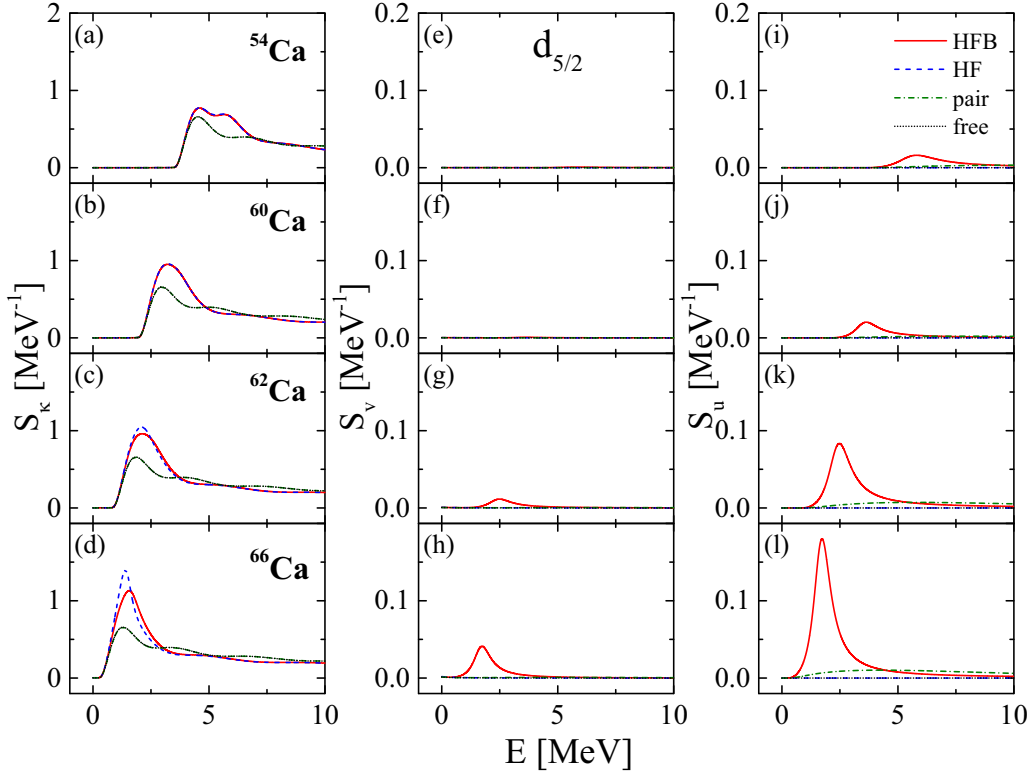
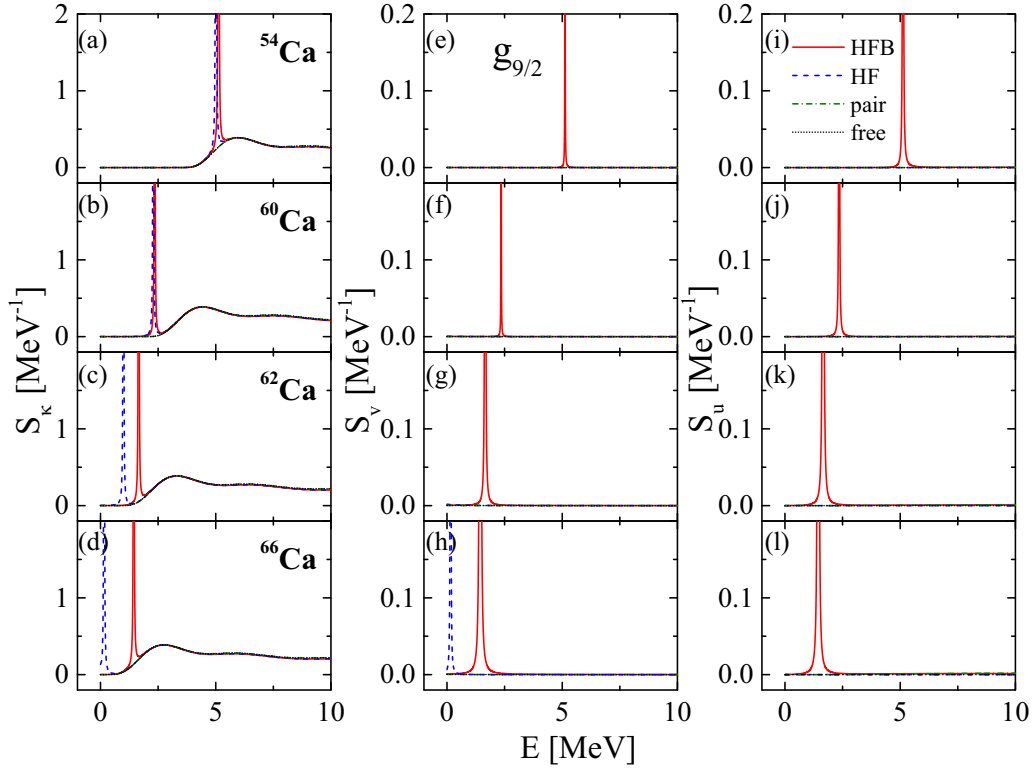FIG. 5. Similar to Fig. 3 but for $d_{5/2}$ partial wave.

From Table I and II, we find that the energy distance between the canonical state $2d_{5/2}$ and the Fermi energy $|\varepsilon_i^{can} - \lambda|$ is quite different from the peak centroid energy read from the HF spectra E_{HF}^{κ}. This is different from the bound single-particle state $2p_{1/2}$. Therefore, the BCS approximation does not work so well for such a state high above in the continuum. However, the shift of peak centroid energy from E_{HF}^{κ} to E_{HFB}^{κ} demonstrates that the resonant energy does increase due to the addition of pairing correlation. This increase is almost invisible in $^{54-58}$Ca but more obvious in $^{60-66}$Ca. This demonstrates again that, the pairing correlation plays a more effective role in the continuum state when this state is closer to the Fermi energy.

In Table II, we found that the peak centroid energies and widths $E_{HFB}^{v}(\Gamma_{HFB}^{v})$ and $E_{HFB}^{u}(\Gamma_{HFB}^{u})$ read from the HFB spectra of occupation probability density S_v and pair probability density S_u for $2d_{5/2}$ partial wave are close to each other. However, their difference with $E_{HFB}^{\kappa}(\Gamma_{HFB}^{\kappa})$ obtained from the quasiparticle-state probability density S_κ are much more obvious. This shows that the resonant energies and widths of such a broad quasiparticle resonance read from different spectra S_κ and S_v (S_u) are not that close with each other, where more continuum coupling is involved due to the pairing correlation.

Actually, for such a single-particle state as $2d_{5/2}$ in the continuum, it may be a single-particle resonance who already has a width in the HF potential, including the centrifugal barrier, which is also called as "shape resonance" [25]. Indeed, the HF spectrum of the density of quasiparticle state S_κ shows a peak with a finite width Γ_{HF}^{κ} even without pairing as listed in Table II. This width should be contributed only from the

HF mean field. One should notice that this single-particle state $2d_{5/2}$ is always above the barrier ($\varepsilon_i^{can} > V_{max}$). As the canonical energy ε_i^{can} falls down while the Fermi energy raises up, the width Γ_{HF}^{κ} first increases a little bit from ^{54}Ca to ^{58}Ca and then quickly decreases up to ^{66}Ca. It is easy to understand that the resonant width reduces as its energy decreases in a potential well with finite depth (see textbook such as Ref. [100]).

Meanwhile, the total width read from the HFB spectra Γ_{HFB}^{κ} of the density of quasiparticle state S_κ first increases in $^{54-58}$Ca, and then decreases to ^{66}Ca, dominated by the change of the width Γ_{HF}^{κ}. From the width's difference $\Delta\Gamma_{pair}^{\kappa}$, we can see that in ^{54,56}Ca, although it is almost negligible, the pairing correlation even reduces the total width. But in $^{62-66}$Ca, the pairing correlation obviously makes the total width increase. Specifically, the contribution only from the pairing correlation $\Delta\Gamma_{pair}^{\kappa}$ grows up to 38% of the total width in ^{66}Ca. Table I mentions that the occupation probability v_i^2 and the factor $u_i v_i$ of the single-particle state $2d_{5/2}$ increase as this state gets closer to the Fermi energy. In ^{66}Ca with the largest $\Delta\Gamma_{pair}^{\kappa}$, the factor $u_i v_i$ also grows up to the largest value. This is similar to what we found in the hole-like quasiparticle resonance originated from $2p_{1/2}$. Therefore, the width of particle-like quasiparticle resonance is also increased due to the pairing correlation, when the state is closer to the Fermi energy. It is also worth noting that the widths read from the HFB spectrum of occupation probability density Γ_{HFB}^{v} and pair probability density Γ_{HFB}^{u} monotonically decrease as the state $2d_{5/2}$ falls down. But we cannot separate the contribution only from the pairing correlation in these spectra due to the lack of the HF spectrum.

FIG. 6. Similar to Fig. 3 but for $g_{9/2}$ partial wave.

4. From unbound to weakly bound: $1g_{9/2}$ state

The quasiparticle spectrum in Fig. 6 shows that there is a sharp peak structure in the HFB spectrum of all the three densities S_κ, S_v, and S_u in $g_{9/2}$ partial wave. The HF spectrum in the density of quasiparticle state S_κ almost coincides with the HFB spectrum in $^{54-60}$Ca in Figs. 6(a) and 6(b), but they separate obviously in $^{62-66}$Ca in Figs. 6(c) and 6(d). The HF spectrum does not appear in the occupation probability density S_v in $^{54-62}$Ca since neutrons cannot occupy this continuum state above the Fermi energy without pairing correlation. But when this state falls down to be weakly bound and below the Fermi energy in ^{66}Ca, it could be occupied and the HF spectrum of S_v suddenly appears in Fig. 6(h).

More explicitly, Table II shows that as the single-particle state $1g_{9/2}$ gets closer to the Fermi energy, the peak of the HF spectrum of S_κ falls below the quasiparticle continuum threshold ($E_{HF}^\kappa < -\lambda$) and becomes a bound quasiparticle state in ^{64,66}Ca. Other peaks of HF spectrum in S_κ and all the peaks of HFB spectrum in S_κ, S_v, S_u represent the quasiparticle resonances above the threshold $-\lambda$. Again, we found the peak centroid energies and widths read from the HFB spectrum of three different densities are almost the same. Besides, the peak centroid energy E_{HF}^κ is close to the energy distance between the canonical state $1g_{9/2}$ and the Fermi energy $|\varepsilon_i^{can} - \lambda|$ as listed in Table I. This is similar to what we found in the bound state $2p_{1/2}$, which shows that the BCS approximation is also robust for this unbound or weakly bound state $1g_{9/2}$. The shift of the peak centroid energy from E_{HF}^κ to E_{HFB}^κ is larger in $^{62-66}$Ca, which shows again that the pairing effects

on the quasiparticle energy is more obvious as this state $1g_{9/2}$ is closer to the Fermi energy.

On the other hand, both the widths Γ_{HF}^κ and Γ_{HFB}^κ read from the HF and HFB spectra of S_κ are rather small. Although the state $1g_{9/2}$ is in the continuum, its width Γ_{HF}^κ is very small since this state is far below its barrier top V_{max}. With the addition of the pairing correlation, the widths Γ_{HFB}^κ are still rather small, even in the most weakly bound nucleus ^{66}Ca. This is obviously different from the state $2d_{5/2}$ much higher above with a smaller pairing gap Δ_i, where the total width is quite large ($\Gamma_{HFB}^\kappa / E_{HFB}^\kappa \approx 70\%$) in ^{66}Ca and the contribution from the pairing correlation $\Delta\Gamma_{pair}^\kappa$ is almost half of the total width.

Therefore, the increase of the quasiparticle resonance width contributed from the pairing correlation is more obvious for the state with smaller angular momentum l.

C. Evolution of quasiparticle resonance as the pairing strength

As we have shown in the previous section, the continuum coupling due to the pairing is the exclusive source of the width for the "hole-like" quasiparticle resonance. But, for the "particle-like" quasiparticle resonance, besides the pairing, the width of single-particle resonance due to the mean field is also one important source of the width. As the mean field changes in different Ca isotopes, the single-particle level changes obviously, leading to the obvious change of the resonant energy and width. In this section, we will focus on one neutron-rich Ca isotope, ^{66}Ca, with the almost-fixed mean

TABLE III. Similar to Table I but for the nucleus ^{66}Ca and the canonical single-particle states $2p_{1/2}$ and $2d_{5/2}$ therein, calculated with different pairing strengths $\eta = 0.66, 0.71, 0.76, 0.80, 0.84$.

	η	0.66	0.71	0.76	0.80	0.84
	λ	−0.234	−0.259	−0.294	−0.324	−0.352
	$\bar{\Delta}$	1.425	1.188	0.998	0.872	0.765
$2p_{1/2}$	$V_{\max}$	0.483	0.486	0.488	0.489	0.490
	$\varepsilon_i^{\mathrm{can}}$	−5.610	−5.686	−5.757	−5.806	−5.849
	$|\varepsilon_i^{\mathrm{can}} - \lambda|$	5.376	5.427	5.463	5.482	5.497
	Δ_i	1.494	1.219	1.001	0.859	0.741
	v_i^2	0.9805	0.9867	0.9909	0.9932	0.9949
	$u_i v_i$	0.1384	0.1144	0.0949	0.0822	0.0714
$2d_{5/2}$	$V_{\max}$	1.719	1.725	1.729	1.732	1.733
	$\varepsilon_i^{\mathrm{can}}$	1.939	1.906	1.888	1.881	1.878
	$|\varepsilon_i^{\mathrm{can}} - \lambda|$	2.173	2.165	2.182	2.205	2.230
	Δ_i	1.282	1.060	0.885	0.772	0.679
	v_i^2	0.0694	0.0509	0.0367	0.0281	0.0217
	$u_i v_i$	0.2541	0.2199	0.1879	0.1653	0.1456

field, and investigate the effects of different pairing strengths on both the "hole-like" and "particle-like" quasiparticle resonances.

Table III shows the same information as in Table I but only for ^{66}Ca and the single-particle states $2p_{1/2}$ and $2d_{5/2}$ therein calculated with different DDDI parameters $\eta = 0.66, 0.71, 0.76, 0.80, 0.84$ in Eq. (4). We can see that the smaller factor η corresponds to a larger pairing strength. Both the average pairing gaps and the state-dependent pairing gaps calculated with $\eta = 0.66$ are almost twice as much as those calculated with $\eta = 0.84$. The Fermi energy is also raised up a little as the pairing correlation becomes stronger. Both the potential barrier tops $V_{\max}$ and the canonical energies remain almost the same as the pairing strengths changes, since they are mainly determined by the HF potential. The occupation probability v_i^2 of the bound single-particle states $2p_{1/2}$ slightly decreases as the pairing strength increases, while that of the unbound single-particle states $2d_{5/2}$ obviously increases. This shows that the stronger pairing correlation can scatter more neutrons from bound to the unbound states.

Accordingly, Table IV shows the same information as in Table II but for $p_{1/2}$ and $d_{5/2}$ partial waves in ^{66}Ca calculated with different pairing strength factors η. The peak centroid energy of the HF spectrum E_{HF}^{κ} of both the two quasiparticle resonances almost remain the same when the pairing strength changes. Again this is because they are determined by the HF potential, which is almost unchanged in the calculation. The peak centroid energy shift from E_{HF}^{κ} to $E_{\mathrm{HFB}}^{\kappa}$ due to the addition of pairing correlation is more obvious calculated with stronger pairing strength.

As we discussed before, for the bound single-particle state $2p_{1/2}$, the total width $\Gamma_{\mathrm{HFB}}^{\kappa}$ of the corresponding hole-like quasiparticle resonance should be all contributed from the pairing correlation. One can clearly see that both the widths $\Delta\Gamma_{\mathrm{pair}}^{\kappa}$ and $\Delta\Gamma_{\mathrm{pair}}^{v}$ are larger in the stronger pairing case. This demonstrates that the stronger pairing correlation does increase the width of the hole-like quasiparticle resonance, which is consistent with the statements in Ref. [71].

For the particle-like quasiparticle resonance originated from the single-particle state $2d_{5/2}$ in the continuum, the width read from the HF spectrum $\Gamma_{\mathrm{HF}}^{\kappa}$ almost remains the same,

TABLE IV. Similar to Table II but only for the peak centroid energy and width read from the quasiparticle spectra of the partial waves $p_{1/2}, d_{5/2}$ in ^{66}Ca, calculated with different pairing strengths $\eta = 0.66, 0.71, 0.76, 0.80, 0.84$.

		S_κ			S_v			S_u
		$E_{\mathrm{HF}}^{\kappa}(\Gamma_{\mathrm{HF}}^{\kappa})$	$E_{\mathrm{HFB}}^{\kappa}(\Gamma_{\mathrm{HFB}}^{\kappa})$	$\Delta\Gamma_{\mathrm{pair}}^{\kappa}$	$E_{\mathrm{HF}}^{v}(\Gamma_{\mathrm{HF}}^{v})$	$E_{\mathrm{HFB}}^{v}(\Gamma_{\mathrm{HFB}}^{v})$	$\Delta\Gamma_{\mathrm{pair}}^{v}$	$E_{\mathrm{HFB}}^{u}(\Gamma_{\mathrm{HFB}}^{u})$
$p_{1/2}$	$\eta = 0.66$	5.188(0.001)	5.405(0.040)	0.039	5.188(0.001)	5.405(0.040)	0.039	5.405(0.040)
	$\eta = 0.71$	5.188(0.001)	5.332(0.020)	0.019	5.188(0.001)	5.332(0.020)	0.019	5.332(0.020)
	$\eta = 0.76$	5.174(0.001)	5.270(0.010)	0.009	5.174(0.001)	5.270(0.010)	0.009	5.270(0.010)
	$\eta = 0.80$	5.157(0.001)	5.227(0.006)	0.005	5.157(0.001)	5.227(0.006)	0.005	5.227(0.006)
	$\eta = 0.84$	5.139(0.001)	5.190(0.004)	0.003	5.139(0.001)	5.190(0.004)	0.003	5.190(0.004)
$d_{5/2}$	$\eta = 0.66$	1.378(0.738)	1.767(1.240)	0.502	—	1.813(0.975)	—	1.803(0.980)
	$\eta = 0.71$	1.406(0.699)	1.647(1.119)	0.420	—	1.737(0.880)	—	1.729(0.881)
	$\eta = 0.76$	1.438(0.688)	1.590(0.977)	0.289	—	1.699(0.817)	—	1.693(0.814)
	$\eta = 0.80$	1.464(0.681)	1.577(0.892)	0.211	—	1.688(0.782)	—	1.682(0.777)
	$\eta = 0.84$	1.490(0.677)	1.577(0.830)	0.153	—	1.687(0.757)	—	1.681(0.750)

since its single-particle energy and the HF potential barrier top $V_{\max}$ do not change so much. However, the width $\Gamma_{\mathrm{HFB}}^{\kappa}$ grows obviously as the pairing strength increases, due to the increase of the contribution from pairing correlation $\Delta\Gamma_{\mathrm{pair}}^{\kappa}$. Meanwhile, we noticed from Table III that with almost the same single-particle energies of $2d_{5/2}$, the larger pairing strengths produce the larger factors v_i^2 and $u_i v_i$, which indicates more neutrons are scattered to this state with stronger pairing. Here it is interesting to mention the similar analysis in Ref. [71] based on the relation between the factor $v_{\mathrm{BCS}}^2/u_{\mathrm{BCS}}^2$ and the width of the particle-like quasiparticle resonance. They found that, at a fixed quasiparticle energy, the larger pairing gap produced the larger $v_{\mathrm{BCS}}^2/u_{\mathrm{BCS}}^2$ (corresponding to a larger $u_i v_i$ in the case of $2d_{5/2}$), indicating the increase of the probability of the quasiparticle state inside the nucleus. This leads to the decrease of the resonance width. Then they concluded that, the pairing correlation could "reduce" the width of the particle-like quasiparticle resonance. This seems to be opposite with our above findings. However, we noticed from Ref. [71] that, with a fixed resonant energy and a larger pairing gap, the corresponding single-particle energy will decrease. This will indeed lead to the reduction of the total width $\Gamma_{\mathrm{HFB}}^{\kappa}$ which is dominated by the decrease of $\Gamma_{\mathrm{HF}}^{\kappa}$ according to our findings in Sec. IIIB3. But, if we look into the contribution from the pairing correlation $\Delta\Gamma_{\mathrm{pair}}^{\kappa}$ separately, we could find that the pairing correlation does increase the total width of this particle-like quasiparticle resonance when it is near the Fermi energy.

IV. SUMMARY

We took the neutron-rich Ca isotopes as examples to investigate the effects of the pairing correlation on the quasiparticle resonant energy and width. The resonant energy and width were read from three kinds of quasiparticle spectra, including the quasiparticle-state probability density, the occupation probability density, and the pair probability density calculated by the self-consistent continuum Skyrme HFB theory with Green's function method. We analyzed in detail the evolution of these quasiparticle spectra and the resonances therein as the Fermi energy approaches zero, and as a function of the pairing strength.

We found that for narrow quasiparticle resonances, the three kinds of quasiparticle spectra calculated with the same potentials can give the same results for the the resonance energy and the width. While for the broad quasiparticle resonances, the difference between the results read from the quasiparticle-state probability density and the occupation probability density or the pair probability density is more obvious.

For the hole-like quasiparticle resonance originated from the bound single-particle states below the Fermi energy, such as $2p_{1/2}$, the pairing correlation is the only source of the resonant width. While for the particle-like quasiparticle resonance corresponding to the unbound single-particle state above the Fermi energy, such as $2d_{5/2}$, the width is contributed from both the HF potential and the pairing correlation. Therefore, the particle-like quasiparticle resonance has much larger resonant width. We tried to separate the pairing correlation's contribution to the total width by comparing the quasiparticle-state probability density calculated with and without the pair potential. We found that the pairing correlation can increase the resonant energy and the width for both the hole-like and particle-like quasiparticle resonances. This increase is larger when the state is closer to the Fermi energy, no matter from below or above. But it is especially obvious for the unbound states with smaller angular momentum l when the Fermi energy approaches zero. Besides, in the $s_{1/2}$ partial wave of the neutron-rich Ca isotopes, although there is no quasiparticle resonance near the continuum threshold, we do find that the pairing correlation can scatter neutrons to the continuum states just above the threshold and make pairs there. This could happen even when the HF potential vanishes, e.g., in the asymptotic region of the neutron-rich nucleus where only the pair potential may remain. This resonant-like increase of occupation in the s wave near the continuum threshold implies that the low-lying nonresonant continuum can have some contribution to the formation of the ground state of the weakly bound nucleus.

[1] I. Tanihata, H. Hamagaki, O. Hashimoto, Y. Shida, N. Yoshikawa, K. Sugimoto, O. Yamakawa, T. Kobayashi, and N. Takahashi, Phys. Rev. Lett. **55**, 2676 (1985).

[2] A. S. Jensen, K. Riisager, D. V. Fedorov, and E. Garrido, Rev. Mod. Phys. **76**, 215 (2004).

[3] B. Jonson, Phys. Rep. **389**, 1 (2004).

[4] J. Meng and S. G. Zhou, J. Phys. G: Nucl. Part. Phys. **42**, 093101 (2015).

[5] J. Dobaczewski, H. Flocard, and J. Treiner, Nucl. Phys. A **422**, 103 (1984).

[6] P. Ring, Prog. Part. Nucl. Phys. **37**, 193 (1996).

[7] J. Meng and P. Ring, Phys. Rev. Lett. **77**, 3963 (1996).

[8] J. Meng, Nucl. Phys. A **635**, 3 (1998).

[9] N. Sandulescu, L. S. Geng, H. Toki, and G. C. Hillhouse, Phys. Rev. C **68**, 054323 (2003).

[10] N. Sandulescu, R. Liotta, and R. Wyss, Phys. Lett. B **394**, 6 (1997).

[11] P. Curutchet, T. Vertse, and R. J. Liotta, Phys. Rev. C **39**, 1020 (1989).

[12] L. G. Cao and Z. Y. Ma, Phys. Rev. C **66**, 024311 (2002).

[13] P. Descouvemont and D. Baye, Rep. Prog. Phys. **73**, 036301 (2010).

[14] J. R. Taylor, *Scattering Theory: The Quantum Theory on Non-relativistic Collisions* (John-Wiley & Sons, New York, 1972).

[15] L. S. Ferreira, E. Maglione, and R. J. Liotta, Phys. Rev. Lett. **78**, 1640 (1997).

[16] I. Hamamoto, Phys. Rev. C **72**, 024301 (2005).

[17] H. T. Fortune, Phys. Rev. C **73**, 014318 (2006).

[18] Z. P. Li, J. Meng, Y. Zhang, S. G. Zhou, and L. N. Savushkin, Phys. Rev. C **81**, 034311 (2010).

[19] Z. P. Li, Y. Zhang, D. Vretenar, and J. Meng, Sci. China Phys. Mech. Astron. **53**, 773 (2010).

[20] B. N. Lu, E. G. Zhao, and S. G. Zhou, Phys. Rev. Lett. **109**, 072501 (2012).

[21] A. U. Hazi and H. S. Taylor, Phys. Rev. A **1**, 1109 (1970).

[22] V. A. Mandelshtam, T. R. Ravuri, and H. S. Taylor, Phys. Rev. Lett. **70**, 1932 (1993).

[23] L. Zhang, S. G. Zhou, J. Meng, and E. G. Zhao, Phys. Rev. C **77**, 014312 (2008).

[24] J. A. Lay, A. M. Moro, J. M. Arias, and J. Gómez-Camacho, Phys. Rev. C **85**, 054618 (2012).

[25] V. I. Kukulin, V. M. Krasnopol'sky, and J. Horáček, *Theory of Resonances: Principles and Applications* (Springer Science & Business Media, B.V., 1989).

[26] G. Cattapan and E. Maglione, Phys. Rev. C **61**, 067301 (2000).

[27] S. C. Yang, J. Meng, and S. G. Zhou, Chin. Phys. Lett. **18**, 196 (2001).

[28] S. S. Zhang, J. Meng, S. G. Zhou, and G. C. Hillhouse, Phys. Rev. C **70**, 034308 (2004).

[29] J. Y. Guo, R. D. Wang, and X.-Z. Fang, Phys. Rev. C **72**, 054319 (2005).

[30] X. D. Xu, S. S. Zhang, A. J. Signoracci, M. S. Smith, and Z. P. Li, Phys. Rev. C **92**, 024324 (2015).

[31] B. Gyarmati and A. T. Kruppa, Phys. Rev. C **34**, 95 (1986).

[32] N. Moiseyev, Phys. Rep. **302**, 212 (1998).

[33] J. Y. Guo, X. Z. Fang, P. Jiao, J. Wang, and B. M. Yao, Phys. Rev. C **82**, 034318 (2010).

[34] Q. Liu, J. Y. Guo, Z. M. Niu, and S. W. Chen, Phys. Rev. C **86**, 054312 (2012).

[35] M. Shi, Q. Liu, Z. M. Niu, and J. Y. Guo, Phys. Rev. C **90**, 034319 (2014).

[36] N. Michel, W. Nazarewicz, M. Płoszajczak, and K. Bennaceur, Phys. Rev. Lett. **89**, 042502 (2002).

[37] N. Li, M. Shi, J. Y. Guo, Z. M. Niu, and H. Z. Liang, Phys. Rev. Lett. **117**, 062502 (2016).

[38] Z. Fang, M. Shi, J. Y. Guo, Z. M. Niu, H. Z. Liang, and S. S. Zhang, Phys. Rev. C **95**, 024311 (2017).

[39] Y. J. Tian, Q. Liu, T. H. Heng, and J. Y. Guo, Phys. Rev. C **95**, 064329 (2017).

[40] S. Shlomo, Nucl. Phys. A **539**, 17 (1992).

[41] S. Shlomo, V. M. Kolomietz, and H. Dejbakhsh, Phys. Rev. C **55**, 1972 (1997).

[42] T. T. Sun, S. Q. Zhang, Y. Zhang, J. N. Hu, and J. Meng, Phys. Rev. C **90**, 054321 (2014).

[43] T. T. Sun, L. Qian, C. Chen, P. Ring, and Z. P. Li, Phys. Rev. C **101**, 014321 (2020).

[44] M. Shi, J. Y. Guo, Q. Liu, Z. M. Niu, and T. H. Heng, Phys. Rev. C **92**, 054313 (2015).

[45] X. X. Shi, M. Shi, Z. M. Niu, T. H. Heng, and J. Y. Guo, Phys. Rev. C **94**, 024302 (2016).

[46] M. Shi, X. X. Shi, Z. M. Niu, T. T. Sun, and J. Y. Guo, Eur. Phys. J. A **53**, 40 (2017).

[47] M. Shi, Z. M. Niu, and H. Z. Liang, Phys. Rev. C **97**, 064301 (2018).

[48] J. Dobaczewski, W. Nazarewicz, T. R. Werner, J. F. Berger, C. R. Chinn, and J. Dechargé, Phys. Rev. C **53**, 2809 (1996).

[49] N. Sandulescu, N. VanGiai, and R. J. Liotta, Phys. Rev. C **61**, 061301(R) (2000).

[50] R. Id Betan, Nucl. Phys. A **879**, 14 (2012).

[51] S. S. Zhang, M. S. Smith, G. Arbanas, and R. L. Kozub, Phys. Rev. C **86**, 032802(R) (2012).

[52] S. S. Zhang, M. S. Smith, Z. S. Kang, and J. Zhao, Phys. Lett. B **730**, 30 (2014).

[53] T. Berggren, Nucl. Phys. A **109**, 265 (1968).

[54] A. T. Kruppa, P. H. Heenen, and R. J. Liotta, Phys. Rev. C **63**, 044324 (2001).

[55] R. I. Betan, N. Sandulescu, and T. Vertse, Nucl. Phys. A **771**, 93 (2006).

[56] K. M. Ding, M. Shi, J. Y. Guo, Z. M. Niu, and H. Z. Liang, Phys. Rev. C **98**, 014316 (2018).

[57] R. Id Betan, Phys. Rev. C **85**, 064309 (2012).

[58] A. Mercenne, N. Michel, J. Dukelsky, and M. Płoszajczak, Phys. Rev. C **95**, 024324 (2017).

[59] M. Lingle and A. Volya, Phys. Rev. C **91**, 064304 (2015).

[60] P. Ring and P. Schuck, *The Nuclear Many-body Problem* (Springer-Verlag, Berlin, 1980).

[61] A. Bulgac, arXiv:nucl-th/9907088v2.

[62] J. Berger, M. Girod, and D. Gogny, Comput. Phys. Commun. **63**, 365 (1991).

[63] J. Meng and P. Ring, Phys. Rev. Lett. **80**, 460 (1998).

[64] J. Meng, I. Tanihata, and S. Yamaji, Phys. Lett. B **419**, 1 (1998).

[65] J. Meng, S. G. Zhou, and I. Tanihata, Phys. Lett. B **532**, 209 (2002).

[66] J. Meng, H. Toki, S. G. Zhou, S. Q. Zhang, W. H. Long, and L. S. Geng, Prog. Part. Nucl. Phys. **57**, 470 (2006).

[67] X. Y. Qu, Y. Chen, S. Q. Zhang, P. W. Zhao, I. J. Shin, Y. Lim, Y. Kim, and J. Meng, Sci. Chin. Phys. Mech. Astron. **56**, 2031 (2013).

[68] X. W. Xia, Y. Lim, P. W. Zhao, H. Z. Liang, X. Y. Qu, Y. Chen, H. Liu, L. F. Zhang, S. Q. Zhang, Y. Kim, and J. Meng, At. Data Nucl. Data Tables **121-122**, 1 (2018).

[69] M. Grasso, N. Sandulescu, N. Van Giai, and R. J. Liotta, Phys. Rev. C **64**, 064321 (2001).

[70] I. Hamamoto and B. R. Mottelson, Phys. Rev. C **68**, 034312 (2003).

[71] Y. Kobayashi and M. Matsuo, Prog. Theor. Exp. Phys. **2016**, 013D01 (2016).

[72] Y. Kobayashi and M. Matsuo, Prog. Theor. Exp. Phys. **2020**, 013D03 (2020).

[73] J. C. Pei, A. T. Kruppa, and W. Nazarewicz, Phys. Rev. C **84**, 024311 (2011).

[74] Y. N. Zhang, J. C. Pei, and F. R. Xu, Phys. Rev. C **88**, 054305 (2013).

[75] K. Mizuyama, N. N. Le, T. D. Thuy, and T. V. Nhan Hao, Phys. Rev. C **99**, 054607 (2019).

[76] N. Michel, K. Matsuyanagi, and M. Stoitsov, Phys. Rev. C **78**, 044319 (2008).

[77] S. T. Belyaev, A. V. Smirnov, S. V. Tolokonnikov, and S. A. Fayans, Sov. J. Nucl. Phys. **45**, 783 (1987).

[78] M. Matsuo, Nucl. Phys. A **696**, 371 (2001).

[79] S. Fayans, S. Tolokonnikov, and D. Zawischa, Phys. Lett. B **491**, 245 (2000).

[80] H. Oba and M. Matsuo, Phys. Rev. C **80**, 024301 (2009).

[81] Y. Zhang, M. Matsuo, and J. Meng, Phys. Rev. C **83**, 054301 (2011).

[82] Y. Zhang, M. Matsuo, and J. Meng, Phys. Rev. C **86**, 054318 (2012).

[83] T. T. Sun, Sci. Sin. Phys. Mech. Astron. **46**, 012006 (2016) [in Chinese].

[84] X. Y. Qu and Y. Zhang, Phys. Rev. C **99**, 014314 (2019).

[85] X. Y. Qu and Y. Zhang, Sci. Chin. Phys. Mech. Astron. **62**, 112012 (2019).

[86] F. Wienholtz, D. Beck, K. Blaum, C. Borgmann, M. Breitenfeldt, R. B. Cakirli *et al.*, Nature **498**, 346 (2013).

[87] D. Steppenbeck, S. Takeuchi, N. Aoi, P. Doornenbal, M. Matsushita, H. Wang *et al.*, Nature **502**, 207 (2013).

[88] S. Michimasa, M. Kobayashi, Y. Kiyokawa, S. Ota, D. S. Ahn, H. Baba *et al.*, Phys. Rev. Lett. **121**, 022506 (2018).

[89] S. Chen, J. Lee, P. Doornenbal, A. Obertelli, C. Barbieri, Y. Chazono *et al.*, Phys. Rev. Lett. **123**, 142501 (2019).

[90] O. B. Tarasov, D. S. Ahn, D. Bazin, N. Fukuda, A. Gade, M. Hausmann *et al.*, Phys. Rev. Lett. **121**, 022501 (2018).

[91] J. Erler, N. Birge, M. Kortelainen, W. Nazarewicz, E. Olsen, A. M. Perhac, and M. Stoitsov, Nature **486**, 509 (2012).

[92] L. Neufcourt, Y. Cao, W. Nazarewicz, E. Olsen, and F. Viens, Phys. Rev. Lett. **122**, 062502 (2019).

[93] K. Bennaceur and J. Dobaczewski, Comput. Phys. Commun. **168**, 96 (2005).

[94] E. Chabanat, P. Bonche, P. Haensel, J. Meyer, and R. Schaeffer, Nucl. Phys. A **635**, 231 (1998).

[95] M. Matsuo, Phys. Rev. C **73**, 044309 (2006).

[96] M. Matsuo, Y. Serizawa, and K. Mizuyama, Nucl. Phys. A **788**, 307 (2007).

[97] G. Audi, F. G. Kondev, M. Wang, W. J. Huang, and S. Naimi, Chin. Phys. C **41**, 030001 (2017).

[98] I. Hamamoto and B. R. Mottelson, Phys. Rev. C **69**, 064302 (2004).

[99] J. A. Lay, C. E. Alonso, L. Fortunato, and A. Vitturi, J. Phys. G **43**, 085103 (2016).

[100] A. Messiah, *Quantum Mechanics Vol. I* (North-Holland, Amsterdam, 1961), p. 397.